Supporting Information

LiF-dominant SEI optimized by Isomerism effect for regulation of Li deposition and LiPS-induced corrosion on the Li anode

Haiou Li[a], Han Zhang [b]， Yangjie Liang [b,*], Guanghui Gu [b]， Chenxin Dong [a], Jianwei Ren [c], Rongfang Wang [b,*], Fusheng Liu [a,b]

[a] School of Intelligent Vehicles and Low-Altitude Emergency Response, Qingdao Hengxing University of Science and Technology, Qingdao, China

[b] College of Chemical Engineering, Qingdao University of Science and Technology, Qingdao, 266042, China

[c] Department of Chemical Engineering, University of Pretoria, cnr Lynnwood Road and Roper Street, Hatfield 0028, South Africa.

*Corresponding author: 2023011029@mails.qust.edu.cn (Y. Liang), rfwang@qust.edu.cn (R. Wang).

1. Experimental Procedures

1.1. Preparation of Carbon Material (NFC):

1 g of peptone was dissolved in 5 mL of deionized water and ultrasonicated for 5–10 min to achieve complete dissolution. The solution was then frozen at –20 °C for 12 h to form ice blocks, followed by lyophilization for 12 h. The resulting dry sample was thoroughly mixed with 10 g of NaCl and ball-milled at 550 rpm for 3 h. The mixture was then subjected to high-temperature carbonization in a tubular furnace under a nitrogen atmosphere, heated at a rate of 5 °C min^{-1} to 900 °C and held for 1 h. After cooling to room temperature, the carbonized product was washed to remove residual salts and dried in an oven at 60 °C, yielding the nitrogen-doped porous carbon (NFC).

1.2. Preparation of Sulfur-Loaded NFC (S@NFC):

NFC and sublimed sulfur were mixed at a mass ratio of 2:3 and ground for 30 min. The mixture was transferred into an argon-filled glovebox and subsequently heated at 155 °C for 12 h to obtain S@NFC.

1.3. Preparation of Li_2S_6 Electrolyte:

Li_2S and sublimed sulfur were combined in a molar ratio of 1:5 and dissolved in a mixed solvent of 1,3-dioxolane (DOL) and dimethoxyethane (DME) (v/v = 1:1). The mixture was stirred at 60 °C for 24 h to obtain a 2 M Li_2S_6 solution.

1.4. Preparation of Electrolyte Additives

The blank electrolyte for lithium–sulfur (Li−S) batteries was prepared using a base solution composed of 1.0 M lithium bis(trifluoromethanesulfonyl)imide (LiTFSI) and 0.1 M $LiNO_3$ dissolved in a 1:1 (v/v) mixture of 1,3-dioxolane (DOL) and dimethoxyethane (DME). Fluoropyridine (FP) was dissolved in the base electrolyte at concentrations of 30, 40, and 50 mM. Electrochemical tests indicated that the 40 mM concentration exhibited the optimal performance. Therefore, all subsequent experiments were conducted using 40 mM FP in the electrolyte.

1.5. Li−S Battery Assembly and Electrochemical Testing

The cathode was prepared by mixing S@NFC (70 wt%), Super P conductive carbon (20 wt%), and polyvinylidene fluoride (PVDF, 10 wt%) binder, which was dissolved in N-methyl-2-pyrrolidone (NMP) to form a uniform slurry. The slurry was then coated onto aluminum foil as the current collector and dried in a vacuum oven at 60 °C for 12 h to remove the solvent. The dried electrodes were punched into circular disks with a diameter of 12 mm, with a typical sulfur mass loading of 1.0–1.4 mg cm^{-2}. Among them, the lithium sheet measures 15.6*0.45mm.

Coin cells (CR2032 type) were assembled in an argon-filled glovebox using the prepared cathodes, lithium metal as the anode, and Celgard 2400 as the separator. All electrochemical measurements referenced the sulfur mass in the cathode for current density and specific capacity calculations (1 C = 1675 mAh g^{-1}). Cells were tested in the voltage range of 1.7–2.8 V using a Neware battery testing system.

Cyclic voltammetry (CV) and electrochemical impedance spectroscopy (EIS) measurements were performed on a CHI 650D electrochemical workstation. CV scans were conducted at sweep rates of 0.1–0.5 mV s^{-1} over the voltage range of 1.7–2.8 V. EIS measurements were carried out in the frequency range of 100 kHz to 10 mHz at

room temperature.

The Li^+ diffusion coefficient (D_{Li^+}) was calculated using the Randles–Sevcik equation:

$$I_p = \left(2.65 \times 10^5\right) \times n^{1.5} \times A \times D_{Li^+} \times C_{Li} \times v^{0.5} \quad (1\text{-}1)$$

where I_p is the peak current (A), n is the number of electrons transferred ($n = 2$), A is the electrode area (1.13 cm^2), C_{Li^+} is the Li^+ concentration in the electrolyte (0.0002 mol cm^{-3}), and v is the scan rate (V s^{-1}).

The Li^+ diffusion coefficient was also evaluated from EIS data using the Warburg factor:

$$D = \frac{R^2T^2}{2A^2n^4F^4C^2\sigma^2}, \qquad Z_{real} = R_e + R_{CT} + \sigma\omega^{-1/2} \quad (1\text{-}2)$$

where R is the gas constant, T is the absolute temperature, A is the electrode area, n is the number of electrons transferred, F is the Faraday constant, C is the Li^+ concentration, σ is the Warburg factor, ω is the angular frequency, R_e is the electrolyte resistance, and R_{CT} is the charge-transfer resistance. All electrochemical tests were conducted at room temperature.

1.6. Physical Characterization

All materials and solvents used in this study were purchased from commercial sources (e.g., Aldrich, Canrd, Dodochem) and used without further purification. The morphology of the prepared materials was examined using a Carl Zeiss Ultra Plus scanning electron microscope (SEM). X-ray photoelectron spectroscopy (XPS) was performed on a British VG Escalab 210 system equipped with an Mg 300 W X-ray source.

1.7. Theoretical Calculations

Density functional theory (DFT) calculations were performed using the B3LYP functional in the Gaussian 09 program, with the 6-31G(d) basis set and Grimme's D3BJ dispersion correction (keywords: em=gd3bj). All structures were fully optimized and verified to have no imaginary frequencies. The highest occupied molecular orbital

(HOMO), lowest unoccupied molecular orbital (LUMO), and electrostatic surface potential (ESP) were analyzed and visualized using Multiwfn and Visual Molecular Dynamics (VMD).

Bond dissociation energies (BDEs) were calculated from the optimized enthalpies of the molecule and its fragments according to the following equation:

$BDE = [H(A\cdot) + H(B\cdot) - H(AB)] \times 628.09$ where $H(AB)$ is the enthalpy of the intact molecule, and $H(A\cdot)$ and $H(B\cdot)$ are the enthalpies of the corresponding radicals, with the resulting BDE expressed in kJ mol^{-1}.

1.8 Mass Measurement Procedure of Lithium Foils After Immersion

- Removal and cleaning: After immersion in lithium polysulfide (LiPS) solution, the lithium foils were carefully retrieved and thoroughly rinsed with anhydrous DOL/DME solvent. This washing procedure was repeated gently to remove residual electrolyte and loosely adhered polysulfide deposits, thereby minimizing the influence of surface contaminants on subsequent mass measurements.
- Drying process: The cleaned lithium foils were transferred into an argon-filled glovebox and allowed to dry naturally. This ensured complete evaporation of residual organic solvents while maintaining strictly inert conditions, thereby preventing any additional oxidation or corrosion induced by exposure to air or moisture.
- Mass measurement: The dried samples were weighed inside the glovebox using an analytical balance with a precision of 0.01 mg.
- Mass loss calculation: The corrosion degree induced by polysulfides was quantified by calculating the mass difference between the pristine lithium foil and the sample after immersion, defined as the initial mass minus the final mass. This value was used as a quantitative metric to evaluate lithium metal degradation caused by LiPS exposure.

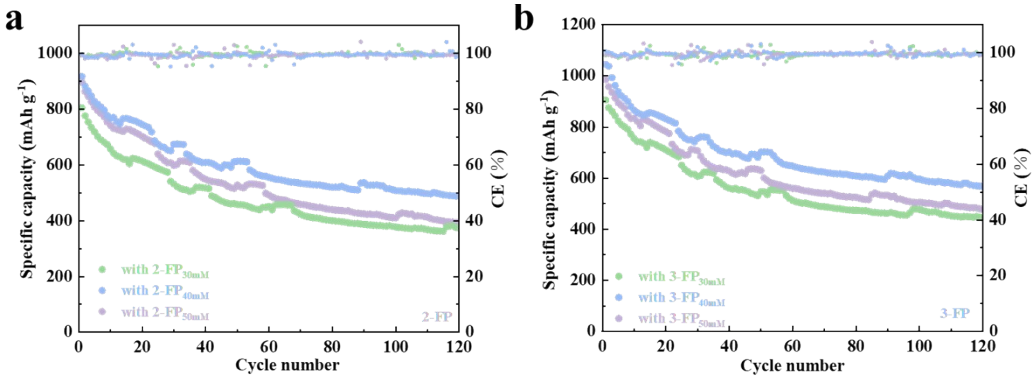

Figure S1. The cycling performance of LSBs at 0.2 C rate with three different concentrations of (a) 2-FP and (b) 3-FP.

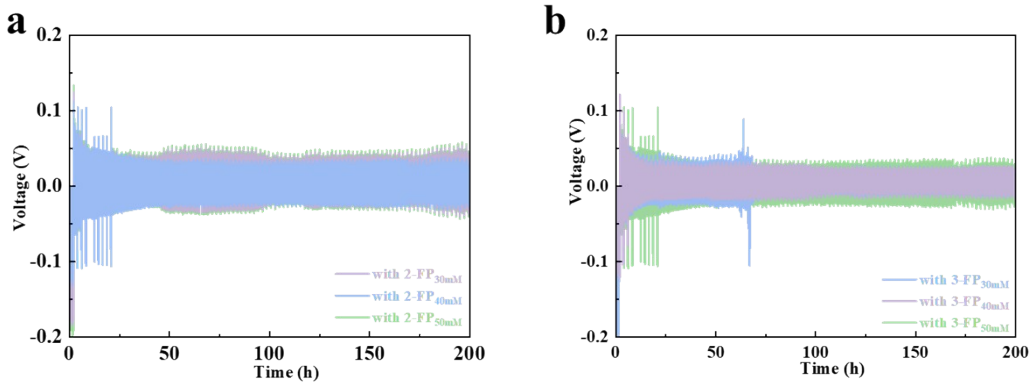

Figure S2. Voltage–time profiles of Li||Li symmetric cells assembled with different concentrations of (a) 2-FP and (b) 3-FP additives.

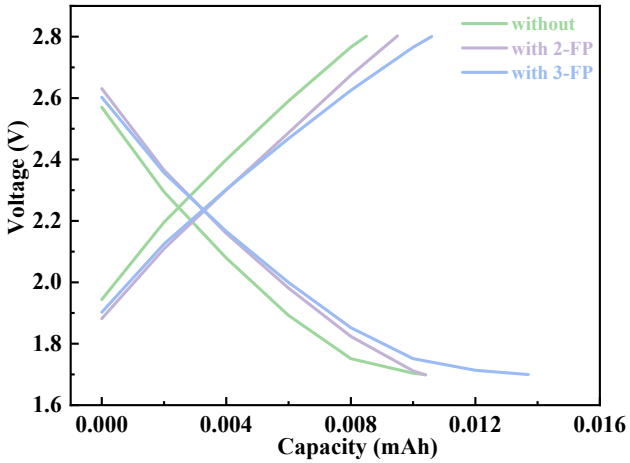

Figure S3. First-cycle charge–discharge profiles at 0.2 C for sulfur-free cells: comparison between the blank electrolyte and cells with fluoropyridine (FP) additives.

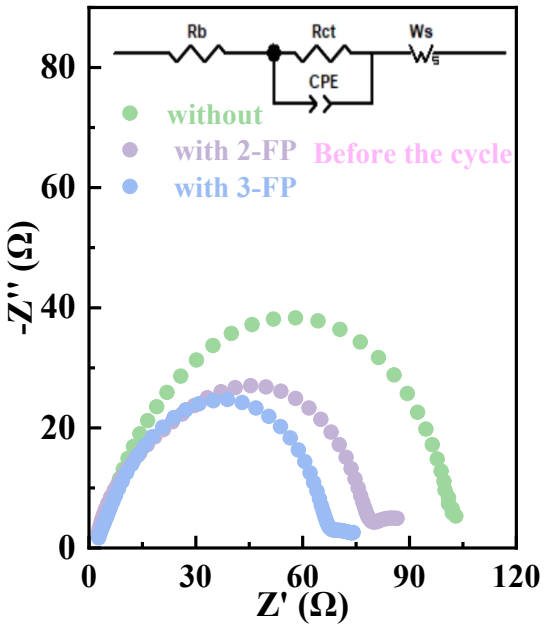

Figure S4. EIS of Li||Li symmetric cells measured before cycling.

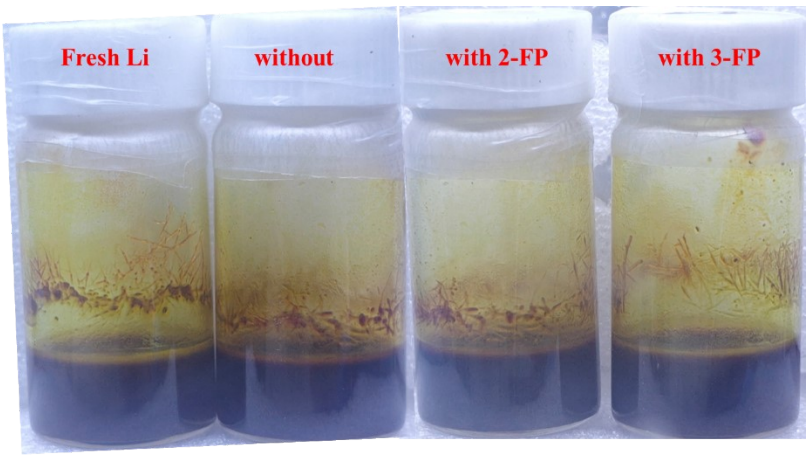

Figure S5. Photographs of fresh lithium and lithium electrodes after the first discharge, immersed in LiPS-containing electrolyte for 30 days.

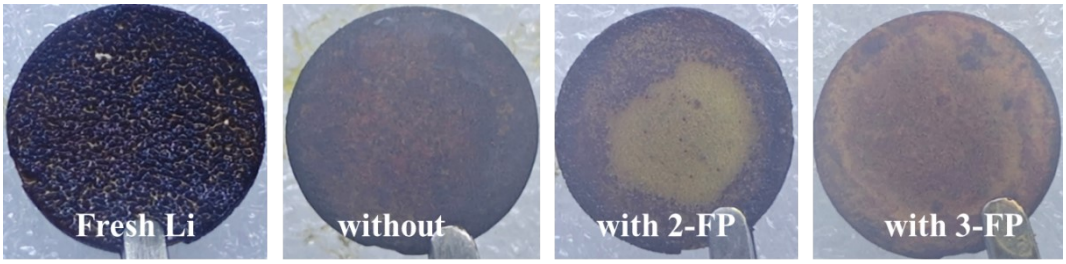

Figure S6. Optical images of fresh lithium and lithium electrodes after the first discharge, following 30-day immersion in LiPS-containing electrolyte.

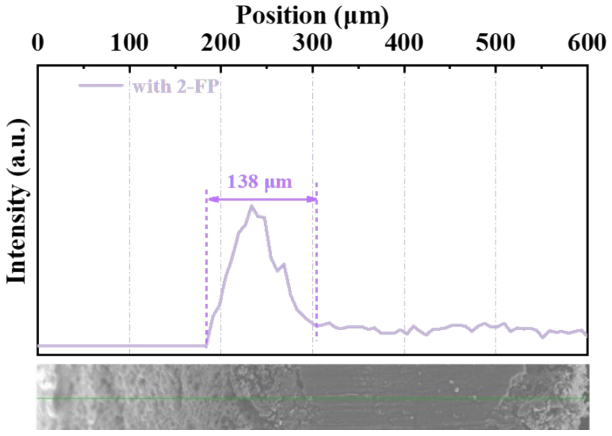

Figure S7. Cross-sectional SEM image of the lithium electrode from the 2-FP additive cell.

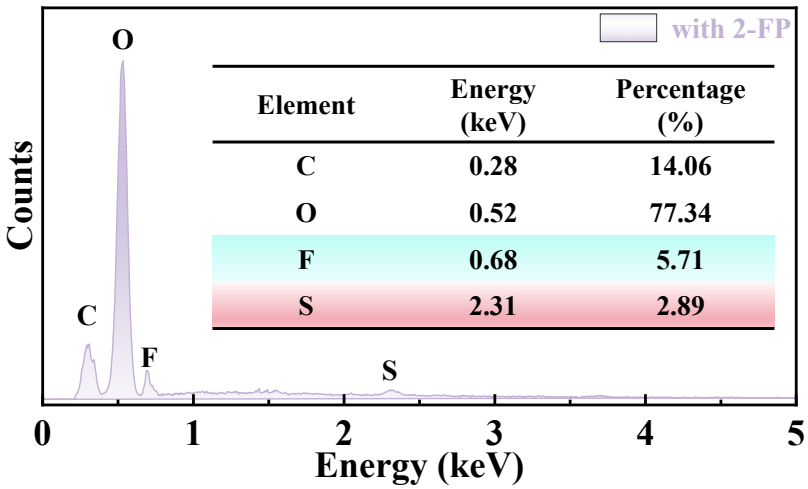

Element	Energy (keV)	Percentage (%)
C	0.28	14.06
O	0.52	77.34
F	0.68	5.71
S	2.31	2.89

Figure S8. Surface EDS mapping of the lithium electrode from the 2-FP additive cell.

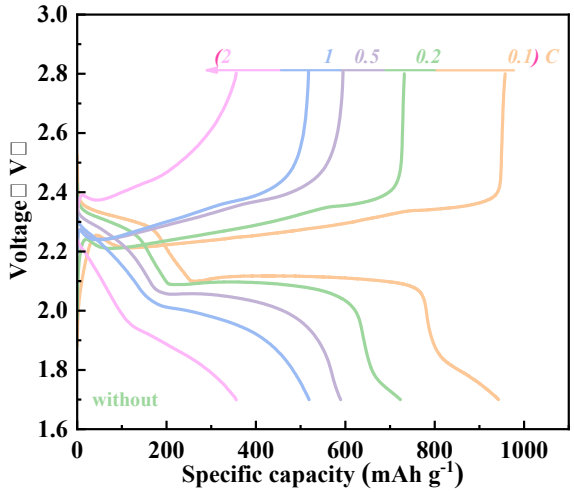

Figure S9. Rate performance charge–discharge curves of the blank Li−S cell.

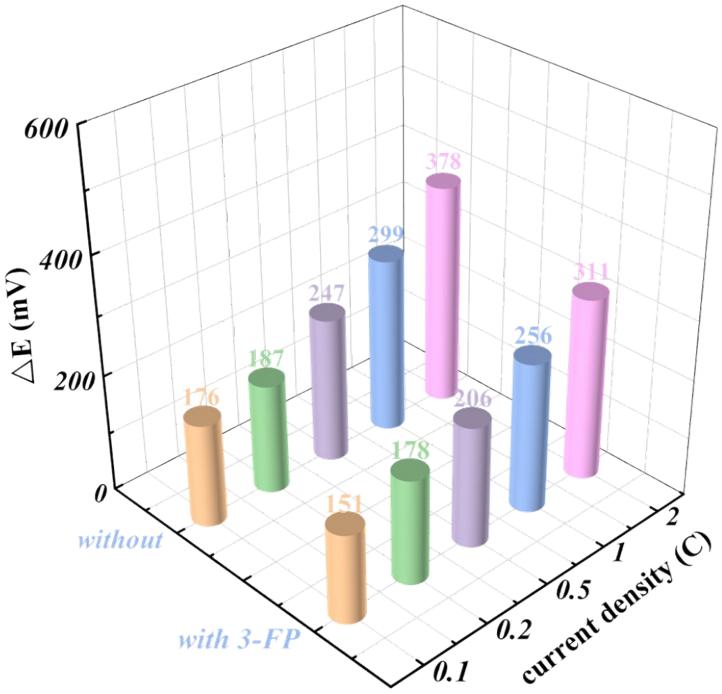

Figure S10. Polarization differences (ΔE) between the blank and 3-FP additive Li−S cells at various current densities.

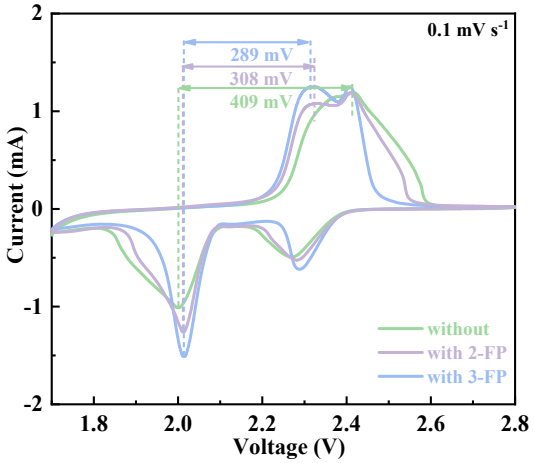

Figure S11. CV curves of the blank and fluoropyridine (2-FP and 3-FP) additive Li−S cells at a scan rate of 0.1 mV s^{-1}.

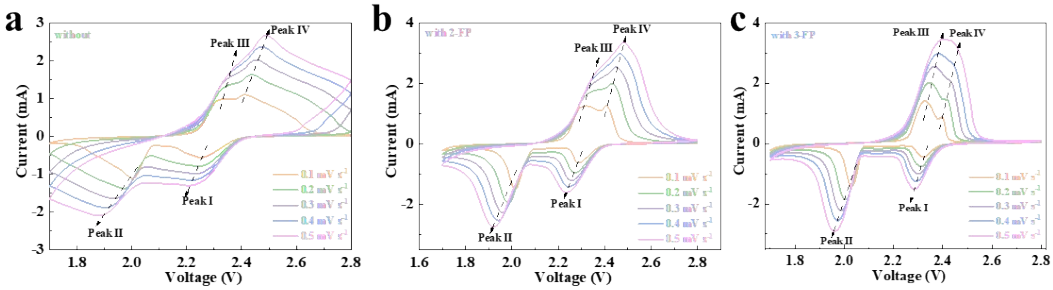

Figure S12. CV curves of blank and fluoropyridine (2-FP and 3-FP) additive Li−S cells at scan rates from 0.1 to 0.5 mV s^{-1}.

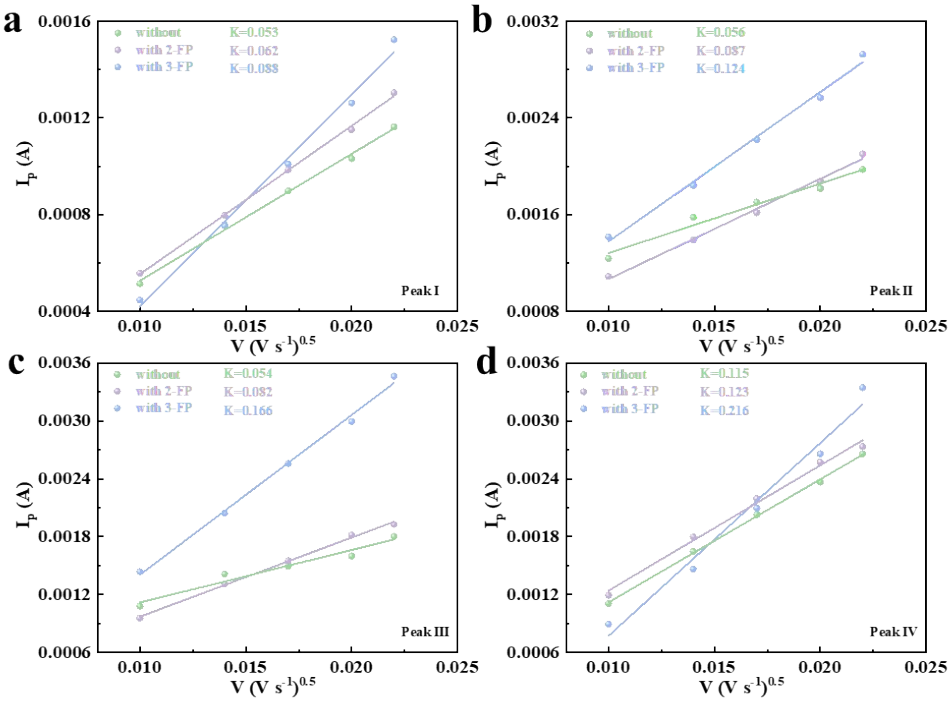

Figure S13. Relationship between Li^+ diffusion coefficients and the square root of scan rates at different redox peak positions for blank and fluoropyridine (2-FP and 3-FP) additive Li−S cells.

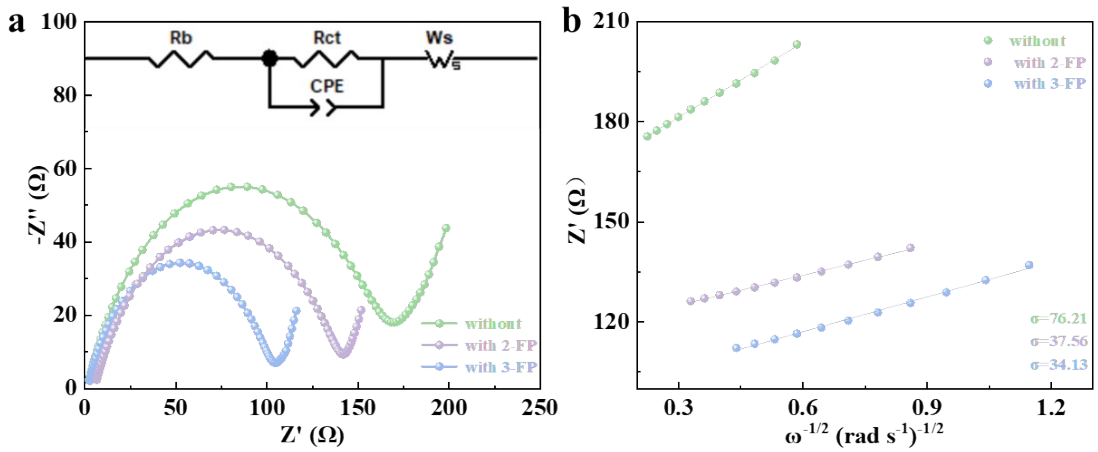

Figure S14. (a) EIS spectra of blank and fluoropyridine (2-FP and 3-FP) additive Li−S cells. (b) Li^+ diffusion resistance derived from EIS fitting using Equation (1-2).

Table S1. Bond lengths and bond angles of fluoropyridine derivatives (2-FP and 3-FP).

	C–F Bond Length (Å)	C–C–F Bond Angle (°)
2-FP	1.343	112.04
3-FP	1.347	119.99

Table S2. Bond dissociation energies (BDEs) of fluoropyridine derivatives.

Reactant (AB)	Radical A	Radical B	BDE (kJ·mol^{-1})
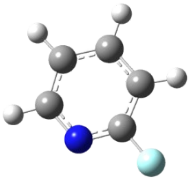	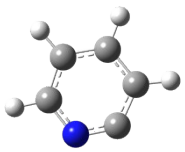		126.1
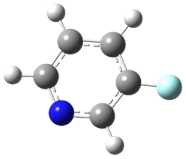	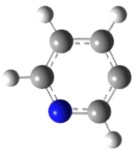		125.8

Table S3. Li^+ diffusion coefficients at different redox peak positions for Li−S batteries with and without fluoropyridine additives.

D_{Li+} ($cm^2\ s^{-1}$)	Peak I ($cm^2 \cdot s^{-1}$)	Peak II ($cm^2 \cdot s^{-1}$)	Peak III ($cm^2 \cdot s^{-1}$)	Peak IV ($cm^2 \cdot s^{-1}$)
Blank	3.68×10^{-9}	4.47×10^{-9}	3.99×10^{-9}	2.23×10^{-8}
with 2-FP	5.01×10^{-9}	9.23×10^{-8}	9.07×10^{-9}	2.36×10^{-8}
with 3-FP	1.05×10^{-8}	2.07×10^{-8}	3.72×10^{-8}	5.45×10^{-8}

Table S4. Performance comparison of Li||Li symmetric cells with various fluorine-containing electrolyte additives.

	SEI component	Current density	Cycle time	Polarized voltage	Reference
LiDFP	Li_3PO_4/LiF	0.1 mA cm^{-2} 0.2 mAh cm^{-2}	1000 h	43 mV	[1]
PFPO	LiF-PO	1 mA cm^{-2} 1 mAh cm^{-2}	1600 h	26 mV	[2]
MgF_2	LiF/LixMg	0.2 mA cm^{-2} —	500 h	110 mV	[3]
PTPEI	LiF	1 mA cm^{-2} —	1000 h	50 mV	[4]
DFAQ	LiF-rich organic-inorganic	1 mA cm^{-2} 1 mAh cm^{-2}	2000 h	18 mV	[5]
1,4-$BzCl_2$	LiCl/LiF	1 mA cm^{-2} 1 mAh cm^{-2}	350 h	50 mV	[6]
3-FP	LiF	0.5 mA cm^{-2} 0.5 mAh cm^{-2}	630 h	23 mV	This work

References:

[1] Yila G, Jia PF, Xia SH, Gong WZ, Song XZ, Zheng TL, et al. Stable Cycling of Solid-State Lithium-Sulfur Batteries by In Situ Construction of Li3PO4/LiF-Enhanced Interface. Acs Applied Materials & Interfaces. 2025;17(47):64542-50.

[2] Chen SY, Meng XD, Han DJ, Chen S, Zhou J, Wang MY, et al. A covalently bonded, LiF-rich solid electrolyte interphase for Li metal batteries with superior low-temperature performance. Chemical Engineering Journal. 2024;500:9.

[3] Duan HH, Liao LP, Bi R, Deng YF, Chen GH. Regulation of polysulfide adsorption and LiF-rich interface chemistry to achieve high-performance PEO-based lithium-sulfur batteries. Journal of Materials Chemistry A. 2023;11(35):19046-55.

[4] Wu T, Jia M, Lu Y, Ye J, Yang D, Zhang Y, et al. Fluorinated imine modulating efficient sulfur redox kinetics and a stable solid electrolyte interphase in lithium–sulfur batteries. Journal of Materials Chemistry A. 2025;13(10):7196-206.

[5] Zhang W, Ma F, Wu Q, Cai Z, Zhong W, Zeng Z, et al. Bifunctional Fluorinated Anthraquinone Additive for Improving Kinetics and Interfacial Chemistry in Rechargeable Li–S Batteries. ACS Applied Energy Materials. 2022;5(12):15719-28.

[6] Li M, Liu Y, Xiao K, Yang S, Sun J, Li S, et al. Steric configuration optimization of dichlorobenzyl additives for enhanced performance of lithium-sulfur batteries. Journal of Power Sources. 2025;658:238350.